

Effects of diamagnetic drift on nonlinear interaction between multi-helicity neoclassical tearing modes

Haiyuan Wang(王海源), Shuai Jiang(姜帅), Tong Liu(刘桐), Lai Wei(魏来), Qibin Luan(栾其斌), and Zheng-Xiong Wang(王正汹)

Citation: Chin. Phys. B, 2024, 33 (**6**): 065202. DOI: 10.1088/1674-1056/ad24d3
Journal homepage: http://cpb.iphy.ac.cn; http://iopscience.iop.org/cpb

What follows is a list of articles you may be interested in

Simulation of deuterium pellet ablation and deposition in the EAST tokamak with HPI2 code

Da-Zheng Li(李大正), Jie Zhang(张洁), Ji-Lei Hou(侯吉磊), Mao Li(李懋), and Ji-Zhong Sun(孙继忠)
Chin. Phys. B, 2024, 33 (**4**): 045204. DOI: 10.1088/1674-1056/ad1e68

Error field penetration in J-TEXT tokamak based on two-fluid drift-MHD model

Wen Wang(王文), Tao Xu(徐涛), Yi Zhang(张仪), and the J-TEXT team
Chin. Phys. B, 2024, 33 (**4**): 045202. DOI: 10.1088/1674-1056/ad1e6b

Numerical study of alpha particle loss with toroidal field ripple based on CFETR steady-state scenario

Niuqi Li(李钮琦), Yingfeng Xu(徐颖峰), Fangchuan Zhong(钟方川), and Debing Zhang(张德兵)
Chin. Phys. B, 2024, 33 (**1**): 015202. DOI: 10.1088/1674-1056/ad03de

Stability impacts from the current and pressure profile modifications within finite sized island

Yuxiang Sun(孙宇翔) and Di Hu(胡地)
Chin. Phys. B, 2023, 32 (**7**): 075212. DOI: 10.1088/1674-1056/acd369

Drift surface solver for runaway electron current dominant equilibria during the current quench

Lu Yuan(袁露) and Di Hu(胡地)
Chin. Phys. B, 2023, 32 (**7**): 075208. DOI: 10.1088/1674-1056/acc1d7

Effects of diamagnetic drift on nonlinear interaction between multi-helicity neoclassical tearing modes

Haiyuan Wang(王海源)[1], Shuai Jiang(姜帅)[1], Tong Liu(刘桐)[1,†], Lai Wei(魏来)[1], Qibin Luan(栾其斌)[2], and Zheng-Xiong Wang(王正汹)[1]

[1] *Key Laboratory of Materials Modification by Laser, Ion, and Electron Beams of the Ministry of Education, School of Physics, Dalian University of Technology, Dalian* 116024, *China*

[2] *Faculty of Electronic Information and Electrical Engineering, Dalian University of Technology, Dalian* 116024, *China*

(Received 25 September 2023; revised manuscript received 23 January 2024; accepted manuscript online 1 February 2024)

A numerical study of the diamagnetic drift effect on the nonlinear interaction between multi-helicity neoclassical tearing modes (NTMs) is carried out using a set of four-field equations including two-fluid effects. The results show that, in contrast to the single-fluid case, 5/3 NTM cannot be completely suppressed by 3/2 NTM with diamagnetic drift flow. Both modes exhibit oscillation and coexist in the saturated phase. To better understand the effect of the diamagnetic drift flow on multiple-helicity NTMs, the influence of typical relevant parameters is investigated. It is found that the average saturated magnetic island width increases with increasing bootstrap current fraction $f_{\rm b}$ but decreases with the ion skin depth δ. In addition, as the ratio of parallel to perpendicular transport coefficients $\chi_{\parallel}/\chi_{\perp}$ increases, the average saturated magnetic island widths of the 3/2 and 5/3 NTMs increase. The underlying mechanisms behind these observations are discussed in detail.

Keywords: tokamak, two-fluid, neoclassical tearing modes, multi-helicity

PACS: 52.55.Fa, 52.30.Cv, 52.35.Py, 52.55.Tn **DOI:** 10.1088/1674-1056/ad24d3

1. Introduction

Macro-scale magnetohydrodynamic (MHD) instabilities are of great significance in the field of magnetic confinement fusion.[1–3] The tearing mode (TM), one kind of the most dangerous instabilities in this context, will occur in the presence of finite resistivity.[4–8] Due to resistive dissipation effects, TMs can alter the topology of the magnetic surfaces through magnetic reconnection, leading to the formation of magnetic islands in the vicinity of rational surfaces. When seed islands in the system reach a sufficient size, the flattening of pressure gradients inside the magnetic islands induces a significant loss of bootstrap current,[9,10] which in turn widens the magnetic islands. This instability is known as the neoclassical tearing mode (NTM) instability.[11] In recent decades, many observations of NTMs have been reported in various experimental devices, including the Tokamak Fusion Test Reactor (TFTR),[11] Joint European Torus (JET),[12] ASDEX Upgrade,[13] Japan Tokamak Upgrade (JT-60U),[14] DIII-D,[15] HL-2A[16] and EAST.[17] In fact, the presence of NTMs poses a serious threat to the operation of tokamak devices. It limits the ability to sustain high-temperature and high-density states in tokamak plasmas. In addition, it causes the expansion and merging of magnetic islands, leading to a loss of energy and greatly reducing the confinement of the device.[15,18–20] In brief, NTMs have detrimental effects on plasma stability and can even result in damage to the device. Therefore, effective control of NTMs is essential to ensure the steady-state operation of tokamak devices.[21–26]

The NTM with a poloidal mode number $m = 3$ and a toroidal mode number $n = 2$ is frequently observed in ASDEX Upgrade, which can lead to energy loss of up to 25% in tokamak plasmas.[27] It is noteworthy that the simultaneous presence of NTMs with different helicities has been observed in experiments conducted on certain tokamak devices.[28–31] These NTMs can coexist and exhibit strong coupling interactions with one another. In addition, the intense interaction among multi-helicity NTMs gives rise to magnetic field stochasticity between two rational surfaces, resulting in severe disruption of magnetic confinement.[32] Li *et al.* discovered that through analytical modeling the nonlinear interaction of TMs with different helicities in cylindrical geometry can happen.[33] Yu *et al.* concluded that the presence of the more unstable magnetic island suppresses the less stable one, which is consistent with the observations in ASDEX Upgrade.[34] Building upon this, Yu *et al.* found that NTMs can be stabilized under the influence of externally applied helical fields with different helicities.[35] Chandra *et al.* numerically simulated the interaction of 3/1 and 2/1 NTMs and observed coupling-induced geodesic acoustic mode (GAM)-like oscillations.[36] Wei *et al.* investigated the coexistence of 3/2 and 2/1 NTMs under different types of plasma rotation and found that they can coexist when plasma rotation is sufficiently large.[37] Liu *et al.* employed electron cyclotron current drive for the control of NTMs and found that NTMs with different helicities can influence each other in the control process.[38]

†Corresponding author. E-mail: liutong@dlut.edu.cn

© 2024 Chinese Physical Society and IOP Publishing Ltd

The previous studies were conducted based on single-fluid theory, but in certain cases single-fluid theory is no longer adequate to explain the physical phenomena observed in tokamak experiments.[39,40] Hence, there has been an increasing focus on research related to two-fluid effects in recent years. For example, studies have been carried out on the control of NTMs by resonant magnetic perturbations,[41–43] on the suppression of the onset of neoclassical double tearing modes by diamagnetic drift,[44] on the systematic numerical simulation of the mode penetration in NTMs,[45] on the influence of Hall effect on TMs[46,47] and on the influence of diamagnetic drift on MHD stability in DIII-D experiments.[48] Despite great progress having been made in two-fluid studies, further research is still required to simulate multi-helicity NTMs based on two-fluid theory.

Therefore, in this study, we numerically investigate the nonlinear interactions between multi-helicity NTMs utilizing the MHD@Dalian code (MD code). It is observed that, unlike in the single-fluid case, the 3/2 NTM is unable to fully suppress the 5/3 NTM and they can coexist during the saturation phase. This phenomenon is attributed to the presence of a sufficiently strong diamagnetic drift flow, which weakens the competitive interaction between the 3/2 and 5/3 NTMs. Moreover, we examined the relationship between the average saturated magnetic island width of the 3/2 and 5/3 NTMs and the bootstrap current fraction, ion skin depth, as well as the parallel and perpendicular transport coefficients. Through detailed discussion of these observed results, the fundamental mechanisms underlying the complex interaction between the diamagnetic drift flow and multi-helicity NTMs are revealed.

2. Model equations

In this paper, the nonlinear evolution of multi-helicity NTMs is investigated by a set of four-field MHD equations that include the two-fluid effect.[49] In order to better simulate the nonlinear evolution of NTMs, it is crucial to include parallel transport terms in the model. The huge difference between the perpendicular and parallel transport coefficients (more than 10^8 order) often leads to severe numerical instability. Thus, fairly high temporal resolution and spatial resolution are required to guarantee the stability of long-time nonlinear evolution of NTMs. In order to limit calculation scale and improve numerical stability, cylindrical geometry is adopted for simplicity.[34,50] It is worth noting that the main difference for the TM between it being in cylindrical geometry and in toroidal geometry is that the favorable curvature effect (so-called GGJ effect)[51] exists in toroidal geometry but not in cylindrical geometry. Curvature effect is indeed significant in a real tokamak configuration. Lütjens *et al.* investigated the influence of plasma curvature on the dynamics of the tearing mode,[52] and their research significantly affects the nonlinear stability threshold of the neoclassical tearing mode. The GGJ effect provides a stabilizing effect on the TM but mainly influences the TM in the linear regime.[53] However, this effect was usually neglected in neoclassical tearing mode dynamics. For large tearing island sizes, the stabilizing effect of GGJ is usually a small quantity in comparison with the drive of perturbed bootstrap current,[54,55] especially in the nonlinear simulation of NTMs. Thus, cylindrical geometry is usually adequate for qualitatively describing nonlinear evolution of NTMs. The modeling of NTMs in cylindrical geometry is widely employed and, according to the significant research conducted using this model, shows promising simulation results. For instance, the simulation results are adopted to explain experimental observations in ASDEX-U[34] and DIII-D.[56] In simulations related to two-fluid dynamics, cylindrical geometry has also been extensively employed.[42,44,45,57] Simulation results have demonstrated the ability to elucidate certain phenomena observed in experiments. Paz-Soldan *et al.* found alignment between simulation results by TM1 code, a nonlinear two-fluid MHD model with cylindrical geometry, and experimental island healing.[58] Nazikian *et al.*, utilizing a nonlinear MHD model in cylindrical geometry, reproduced the experimental observations of pedestal collapse in DIII-D.[59] Hu *et al.* revealed that the simulation results from a nonlinear two-fluid MHD model in cylindrical geometry almost perfectly match the experimental observations in the DIII-D tokamak.[60] Moreover, numerical simulations have revealed that in DIII-D, employing higher toroidal mode number RMPs can achieve a broader window of ELM suppression at high pedestal pressures. This finding provides a crucial reference value for the DIII-D M-coil upgrade. Apparently, the cylindrical geometry model continues to be an effective tool for addressing issues associated with two-fluid dynamics. Thus, it is currently a robust tool that is capable of qualitatively dealing with the NTM-related problems, as well as two-fluid dynamics.

Here, the normalized equations in cylindrical geometry (r,θ,z) are as follows:

$$\frac{\partial U}{\partial t} = [U,\phi+\delta\tau p]+\nabla_{\parallel} j+\nu\nabla_{\perp}^2 U+\delta\tau[\nabla_{\perp} p,\nabla_{\perp}\phi], \quad (1)$$

$$\frac{\partial \psi}{\partial t} = -\nabla_{\parallel}\phi+\beta_{\rm e}\delta\nabla_{\parallel} p-\eta\,(j-j_{\rm b}), \quad (2)$$

$$\frac{\partial p}{\partial t} = [p,\phi]+2\beta_{\rm e}\delta\nabla_{\parallel} j-\beta_{\rm e}\nabla_{\parallel} v+\chi_{\parallel}\nabla_{\parallel}^2 p+\chi_{\perp}\nabla_{\perp}^2 p, \quad (3)$$

$$\frac{\partial v}{\partial t} = [v,\phi]-\frac{1}{2}(1+\tau)\nabla_{\parallel} p+\mu\nabla_{\perp}^2 v, \quad (4)$$

where ψ, ϕ and p are magnetic flux, stream function and pressure, respectively. $U=\nabla^2\phi$ and $j=-\nabla^2\psi$ represent the vorticity and plasma current density along the axial direction, respectively. v is the parallel ion velocity. $\tau=T_{\rm i}/T_{\rm e}$

is the ratio of ion temperature to electron temperature. $\delta = (2\Omega_{\rm i}\tau_a)^{-1}$ is the ion skin depth, where $\Omega_{\rm i} = eB_0/m_{\rm i}$ is the ion gyrofrequency and $\tau_a = \sqrt{\mu_0\rho}a/B_0$ is Alfvén time. The equilibrium electron diamagnetic flow is determined to be $v_{\rm dia0} = -\delta\partial p_0/\partial r$. $\nu = \tau_a/\tau_\nu$ and $\eta = \tau_a/\tau_\eta$ in Eqs. (1) and (2) denote the viscosity and resistivity, respectively. Here, $\tau_\nu = a^2/\hat{\mu}$ and $\tau_\eta = a^2\mu_0/\hat{\eta}$ are, respectively, the viscosity diffusion time and resistive diffusion time ($\hat{\mu}$ and $\hat{\eta}$ are the actual viscosity and resistance). The bootstrap current in Eq. (2) is given by $j_{\rm b} = -A\sqrt{\varepsilon}/B_\theta p'(r)$, where B_θ represents the poloidal magnetic field, and $\varepsilon = r/R_0$ denotes the inverse aspect-ratio. After normalizing r by a, the relationship between $j_{\rm b}$ and ε is $j_{\rm b}\propto\alpha(\hat{r})\sqrt{\hat{r}a/R_0} = \alpha(\hat{r})\sqrt{\hat{r}}\sqrt{a/R_0} = A(\hat{r})\sqrt{\varepsilon}$ where $\varepsilon = a/R_0$. It is important to note that ε includes radial information, with r incorporated into the function $A(\hat{r})$, encompassing radial distribution in our model. A is a constant that can be determined based on the given expression for bootstrap current fraction $f_{\rm b} = \int_0^a j_{\rm b}r{\rm d}r/\int_0^a jr{\rm d}r$. The expression $\beta_{\rm e} = 2\mu_0 n_0 T_{\rm e}/B_0^2$ represents the ratio of thermal pressure to magnetic pressure. $\chi_\parallel$ and $\chi_\perp$, normalized by a^2/τ_a, are denoted as parallel and perpendicular transport coefficients, respectively. Time t, velocity v and the radial coordinate r are scaled using Alfvén time τ_a, Alfvén velocity $v_{\rm A} = B_0/\sqrt{\mu_0\rho}$, and the plasma minor radius a, respectively. μ is the diffusion coefficient of parallel ion velocity normalized by a^2/τ_a. The poloidal magnetic flux ψ, electric potential ϕ and plasma pressure p are normalized by aB_0, $aB_0v_{\rm A}$ and the pressure at the magnetic axis, respectively. The Poisson brackets in Eqs. (1)–(4) are defined as $[f,g] = \hat{z}\cdot\nabla f\times\nabla g$. The parallel gradient operator is defined as $\nabla_\parallel S = [S,\psi] + \partial S/\partial z = \hat{z}\cdot\nabla S\times\nabla\psi + \partial S/\partial z$.

Each variable $f(r,\theta,z,t)$ in Eqs. (1)–(4) can be expressed in the form $f = f_0 + \tilde{f}(r,\theta,z,t)$ with f_0 and $\tilde{f}$ being the time-independent initial profile term and time-dependent perturbation term, respectively. Through the application of the periodic boundary conditions in both the poloidal and axial directions, the perturbed fields can be subjected to Fourier transformation, yielding

$$\tilde{f}(r,\theta,z,t) = \frac{1}{2}\sum_{m,n}\tilde{f}_{m,n}(r,t)\exp({\rm i}m\theta - {\rm i}nz/R_0), \tag{5}$$

with R_0 being the major radius of the tokamak. Utilizing the initial value code, MD code, equations (1)–(4) can be solved based on the provided initial profiles. The radial direction employs the finite difference method, while the angular direction employs the pseudo-spectral method. For time advancement, a two-step prediction–correction method is employed.

The radial boundary condition is considered with an ideal conducting wall, specified as $\tilde{\psi}_{m,n}(r=1) = 0$. The initial safety factor q-profile chosen in this study is shown in Fig. 1. The radial discretization is defined with $N_{\rm r} = 1000$ grid points. Unless otherwise specified, other crucial parameters are set as $\varepsilon = a/R_0 = 0.25$, $\chi_\parallel = 10$, $\chi_\perp = 5\times10^{-6}$, $\eta = 9\times10^{-7}$, $\upsilon = 5\times10^{-6}$ and $\beta_{\rm e} = 0.01$. To ensure stability in the multi-helicity nonlinear calculation for the static equilibrium with $v_0(r) = 0$, the dominant resonant modes with low mode numbers ($0\le m\le 10, 0\le n\le 6$) are specifically chosen.

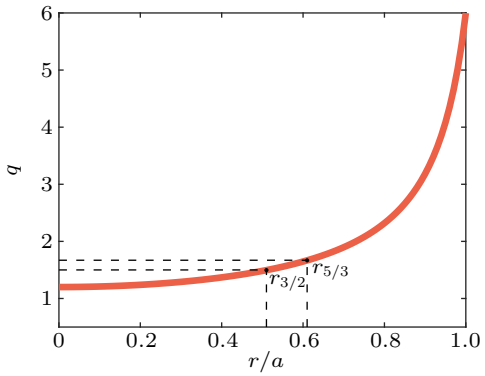


Fig. 1. The initial monotonic safety factor q-profile.

3. Numerical results

To begin with, the effect of the diamagnetic drift on the nonlinear evolution of island width, for single-helicity simulations, is investigated. Different magnitudes of diamagnetic drift flow can be obtained by varying the value of δ. As shown in Fig. 2(a), the width of a saturated magnetic island decreases with increasing δ, indicating that the diamagnetic drift flow has a stabilizing effect on the magnetic island. Notably, for $\delta = 2\times10^{-4}$, oscillation is observed in the magnetic island. The occurrence of oscillation results from the negative feedback regulation between $\beta_{\rm e}\delta\nabla_\parallel p$ in Eq. (2) and the magnetic island width.[45] Figure 2(b) gives the dependence of average saturated magnetic island width on δ. In this context, "average" refers to the mean value of the magnetic island width during the saturation phase, considering the periodic oscillations observed in the magnetic island width. The average island width decreases with the increase in δ. Due to the stabilizing effect of the diamagnetic drift flow, the larger the value of δ, the smaller the average island width. However, it is found that when δ is sufficiently large, the average saturated magnetic island width remains almost unchanged as δ increases, showing a flat average saturated magnetic island width region of δ. The evolution of the saturated magnetic island width with different δ values within the flat region is given in Fig. 3(a), clearly demonstrating that the oscillation amplitude of the magnetic island decreases in response to increasing δ. When δ exceeds a threshold, the suppressing effect of $\beta_{\rm e}\delta\nabla_\parallel p$ decouples from the magnetic island width and the oscillation disappears. Figure 3(b) illustrates that the oscillation frequency is kept nearly constant for changing δ, which indicates that δ has no effect on the oscillation frequency of the magnetic island.

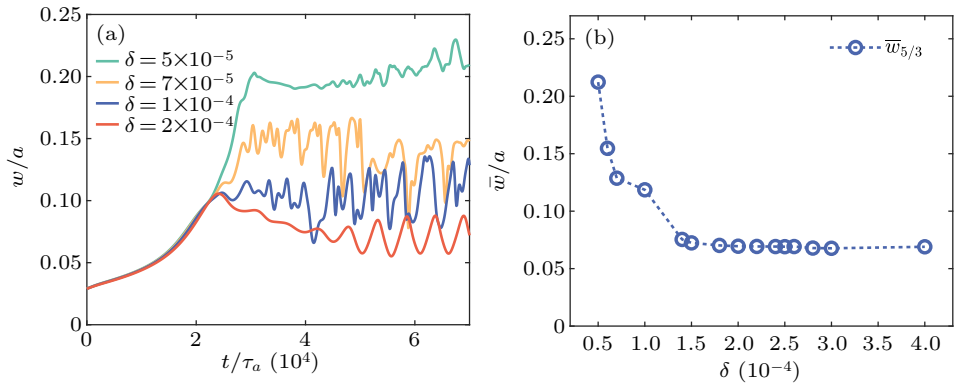


Fig. 2. (a) The temporal evolution of island width of 5/3 NTMs in single-helicity simulations with various δ cases under $f_b = 0.5$. (b) The average saturated magnetic island width versus δ.

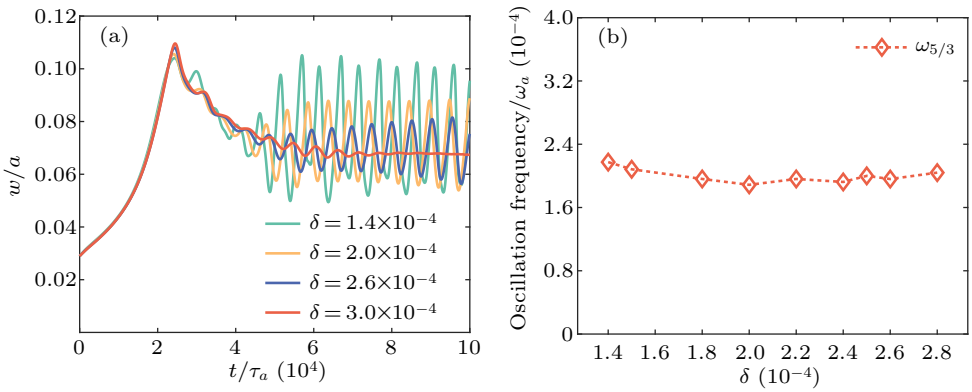


Fig. 3. (a) The temporal evolution of island width of 5/3 NTMs in single-helicity simulations for different δ cases under $f_b = 0.5$. (b) The oscillation frequency versus δ.

Here, simulations of multi-helicity NTMs both in single-fluid and two-fluid models are discussed separately. Based on the single-fluid theory, it is found that the 5/3 NTM is completely suppressed when the magnetic island width of the 3/2 NTM exceeds that of the 5/3 NTM. The presence of the 3/2 NTM strengthens the radial magnetic field, thereby enhancing the perpendicular transport across the 5/3 rational surface. This, in turn, weakens the influence of the bootstrap current on the 5/3 NTM and ultimately leads to the suppression of the 5/3 NTM. Similar findings have been reported in previous studies.[34,37,38] In contrast, the effects of diamagnetic drift flow on simulations of multi-helicity NTMs are examined in Fig. 4(a). Unlike the previous case, the 5/3 NTM in this case is not fully suppressed by the presence of 3/2 NTM. Instead, both modes oscillate together and almost reach an equal magnetic island width after a period of time. When diamagnetic drift flow is sufficiently strong, the competitive effect between the 3/2 and 5/3 NTMs is weakened, allowing for their coexistence during the saturation phase.[37] Furthermore, Figs. 4(b)–4(d) present the nonlinear evolution of kinetic energy, magnetic energy and island width for NTMs with different poloidal mode numbers, including m/n= 3/2, 5/3, 6/4, 8/5, 9/6 and 10/6. It is observed that as the poloidal mode number increases, the amplitudes of kinetic energy, magnetic energy and magnetic island width decrease for NTMs with the same helicity. The fundamental harmonic mode is found to be the most unstable, while higher-order harmonic modes are relatively less unstable. The figures also demonstrate the nonlinear evolution of the 8/5 NTM.

Figure 5 describes the mode structure of the flux perturbation at typical moments. During the early stage, only the 5/3 NTM is present in the system, as shown in Fig. 5(a). After introducing 3/2 NTM, the 5/3 NTM is suppressed on some level. At this point, the width of the 3/2 NTM is larger than that of the 5/3 NTM shown in Fig. 5(b), indicating that the 3/2 mode plays the dominant role. In the saturation phase (t = 72800 and t = 83400), the widths of the 3/2 NTM and 5/3 NTM are comparable, and thus the nonlinear dynamic of the system is determined by the strong interaction between the 3/2 and 5/3 NTMs. To better understand the mechanism behind the interaction of the multi-helicity NTMs, Poincaré plots of magnetic field lines are given in Fig. 6, which also present the four specific moments depicted in Fig. 5. These plots visually illustrate the spatial distribution and behavior of the magnetic field lines, directly exhibiting the evolution of the magnetic topology during the nonlinear interactions of the multi-helicity NTMs. Figure 6(a) shows that there are five magnetic islands evenly located at the 5/3 rational surface. After introducing the 3/2 NTM, a chain of magnetic islands appears at the 3/2 rational surface, as depicted in Fig. 6(b). Moreover, as shown in Figs. 6(c) and 6(d), the chains of magnetic islands for both the 3/2 and 5/3 NTMs are observable, and their sizes are comparable. The intense coupling between the 5/3 mode and the 3/2 mode results in the emergence of strong magnetic stochasticity.

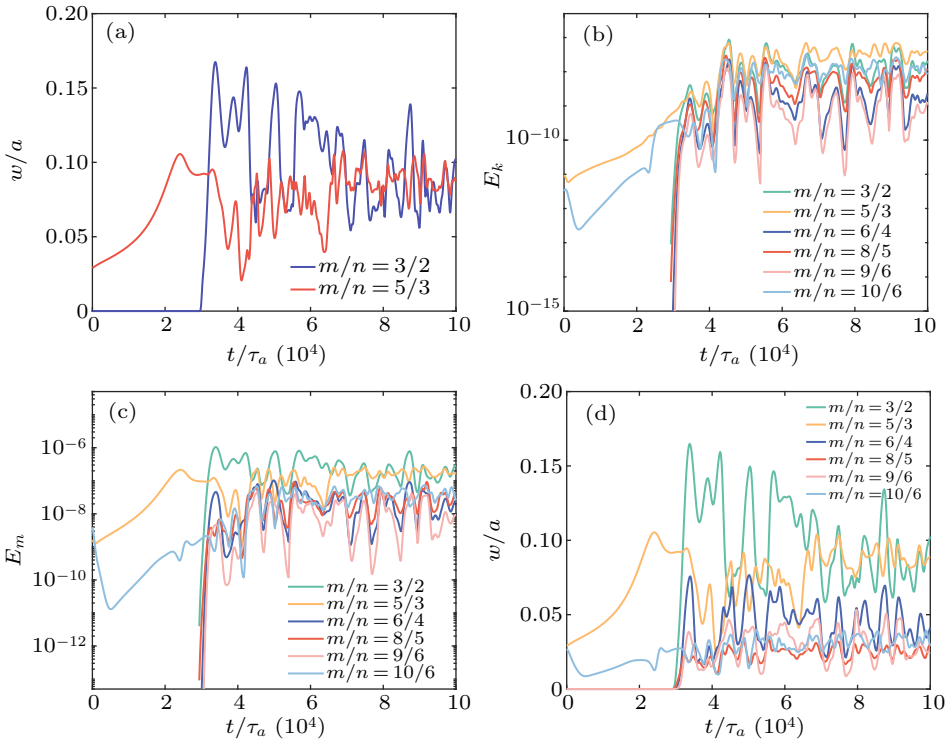


Fig. 4. (a) Time evolutions of magnetic island width of the 3/2 and 5/3 NTMs in multi-helicity simulations with $\beta_e = 0.01$, $\delta = 2 \times 10^{-4}$ and $f_b = 0.5$. Time evolutions of (b) kinetic energy, (c) magnetic energy and (d) island width of $m/n = 3/2$, 5/3, 6/4, 8/5, 9/6, 10/6 NTMs.

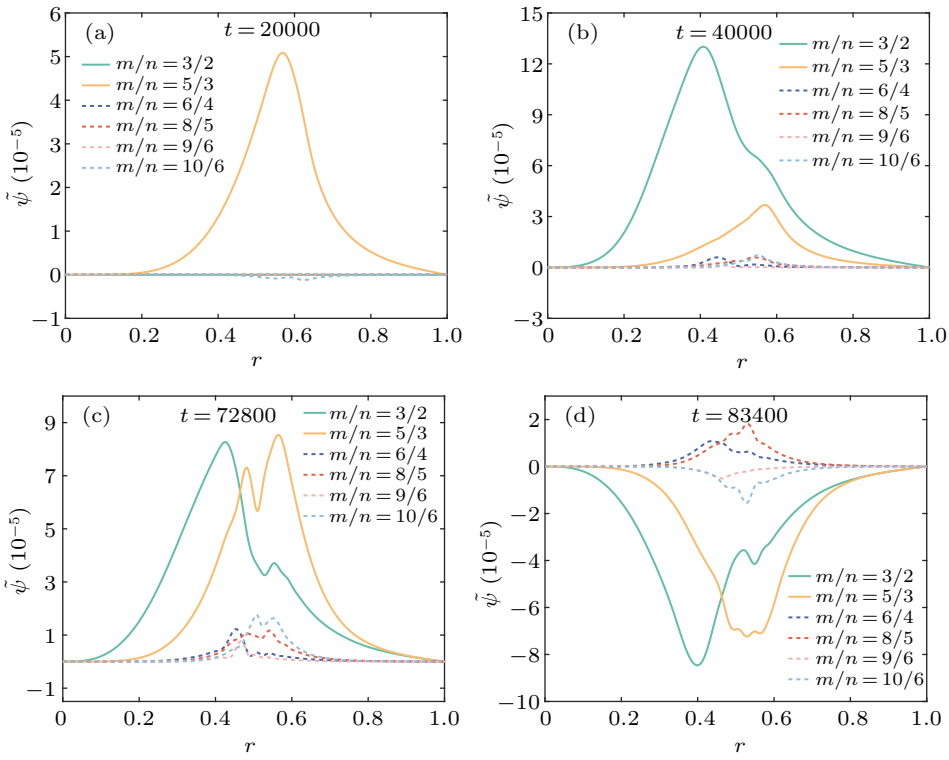


Fig. 5. Typical mode structure of the flux perturbation of $m/n = 3/2$, 5/3, 6/5, 8/5, 9/6, 10/6 NTMs at (a) $t = 20000$, (b) $t = 40000$, (c) $t = 72800$ and (d) $t = 83400$ in Fig. 4(a).

To better understand the two-fluid effects on multi-helicity NTMs, the impact of critical plasma parameters on multi-helicity NTMs is investigated. Figure 7(a) demonstrates that the average saturation island width of 3/2 and 5/3 NTMs increases with the increase in bootstrap current fraction f_b. For higher values of f_b, the stronger destabilizing effect of perturbed bootstrap current on multi-helicity NTMs leads to larger magnetic island width. It is observed that the magnetic island widths of 5/3 NTM and 3/2 NTM always remain comparable while changing f_b in the investigated region in this study. The dependence of the average saturated magnetic island width of 3/2 and 5/3 NTMs on parameter δ is displayed in

Fig. 7(b). Different from the single-helicity simulations shown in Fig. 2(b), the flat region of saturated width does not exist in multi-helicity cases. Due to the profile effect, the diamagnetic drift flow has different influence on different helicity NTMs. The existence of multi-helicity NTM islands will in turn affect the nonlinear evolution of diamagnetic drift flow. Thus, the flat region observed in single-helicity simulation is hard to find when the multi-helicity coupling effect is considered. In Figs. 8(a) and 8(b), the influence of the parallel transport and perpendicular transport coefficients on the island width are respectively investigated. Other parameters are set as $f_{\rm b}=0.6$, $\eta=1.9\times10^{-6}$, $\upsilon=5\times10^{-6}$, $\beta_{\rm e}=0.01$ and $\delta=3\times10^{-4}$. The parallel transport coefficient $\chi_{\parallel}$ and perpendicular transport coefficient $\chi_{\perp}$ have opposite effects on the stability of multi-helicity NTMs. An increased ratio of $\chi_{\parallel}/\chi_{\perp}$ can enhance the transport along the magnetic field lines, reinforcing the loss of the bootstrap current and further destabilizing the magnetic island. Consequently, it can be seen that a larger (smaller) perpendicular (parallel) transport coefficient results in a larger island width.

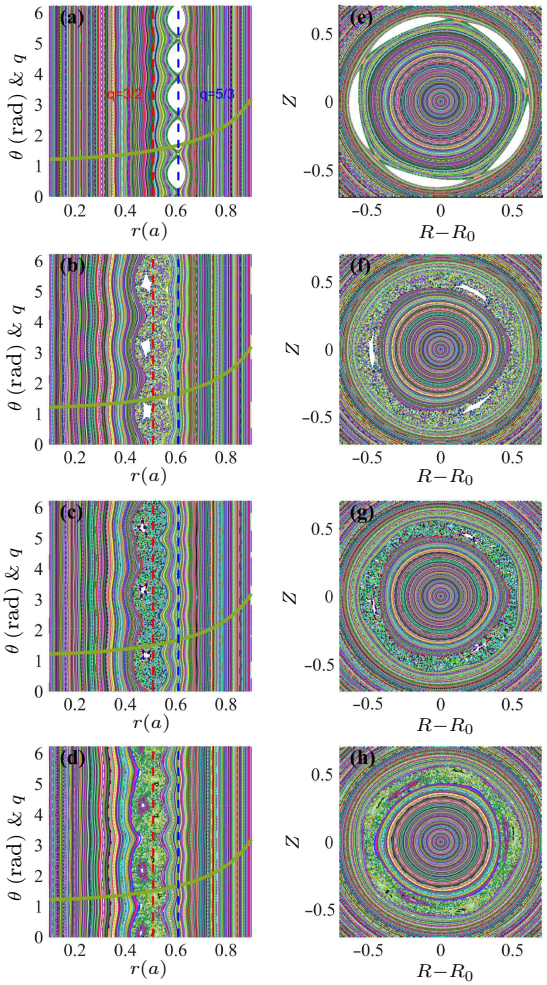


Fig. 6. From the first row to the fourth row, Poincaré plots of magnetic field lines in a poloidal cross section $(r,\theta,\xi=0)$ are displayed at the corresponding moments shown in Fig. 5: (a)–(d) rectangular plan $(r,\theta)\rightarrow(x,y)$; (e)–(h) circular plan $(r,\theta)\rightarrow(R-R_0,Z)$ with $R=R_0+r\cos\theta$ and $Z=r\sin\theta$.

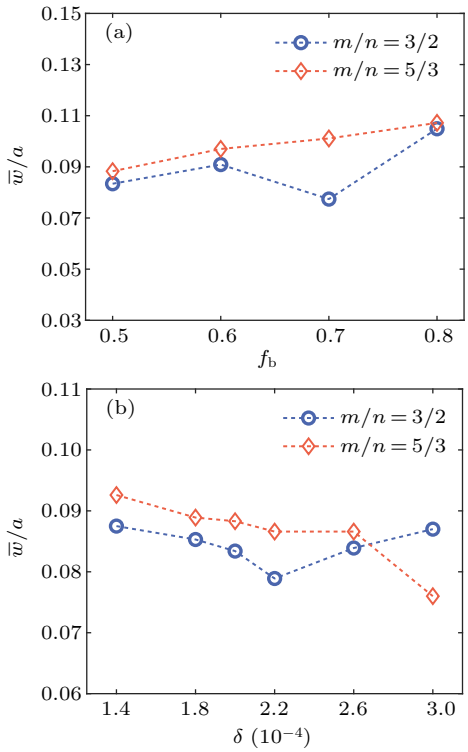


Fig. 7. Average saturated magnetic island width for the 3/2 and 5/3 NTMs as a function of (a) bootstrap current fraction $f_{\rm b}$ with $\delta=2\times10^{-4}$ and (b) ion skin depth δ with $f_{\rm b}=0.5$.

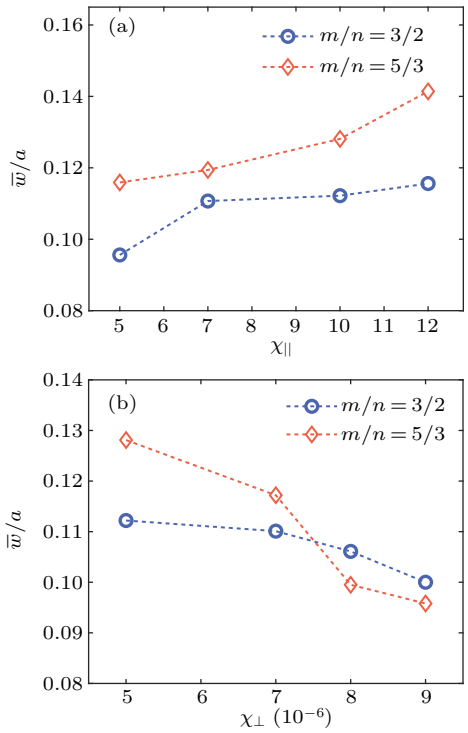


Fig. 8. Average saturated magnetic island width for the 3/2 and 5/3 NTMs as a function of (a) parallel transport coefficient $\chi_{\parallel}$ and (b) perpendicular transport coefficient $\chi_{\perp}$. Other parameters are set as $f_{\rm b}=0.6$, $\eta=1.9\times10^{-6}$, $\upsilon=5\times10^{-6}$, $\beta_{\rm e}=0.01$ and $\delta=3\times10^{-4}$.

4. Conclusion

In this study, we have conducted a numerical investigation into the impact of diamagnetic drift effect on the nonlinear interaction between multi-helicity NTMs. The study is

based on a set of four-field equations that include two-fluid effects. Our findings reveal that the presence of diamagnetic drift flow weakens the nonlinear interaction between multi-helicity NTMs. Specifically, the stabilizing effect of the 3/2 NTM on the 5/3 NTM is reduced compared to the single-fluid results, so that the 5/3 NTM is not completely suppressed. The average saturated magnetic island width of the multi-helicity NTMs increases with an increase in the bootstrap current fraction $f_{\rm b}$, which has a destabilizing effect. In contrast, the average saturated magnetic island width decreases with an increase in the ion skin depth δ (which represents the magnitude of the diamagnetic drift flow), indicating a stabilizing effect. In addition, a higher ratio of parallel to perpendicular transport coefficients $\chi_{\parallel}/\chi_{\perp}$ leads to an increased magnetic island width by enhancing pressure transport along the magnetic field lines.

In this study, numerical investigation reveals the basic process of nonlinear interaction between multi-helicity NTMs with diamagnetic drift flow. However, it is important to note that, for simplicity, the effect of $\boldsymbol{E}\times\boldsymbol{B}$ shear flow has not been considered in this study. $\boldsymbol{E}\times\boldsymbol{B}$ shear flow also has a stabilizing effect on NTMs, and further research may investigate the synergistic effects of both diamagnetic drift flow and $\boldsymbol{E}\times\boldsymbol{B}$ shear flow on NTMs in the future.

Acknowledgements

The authors acknowledge the Supercomputer Center of Dalian University of Technology for providing computing resources.

Project supported by the National Key R&D Program of China (Grant No. 2022YFE03090000), the National Natural Science Foundation of China (Grant Nos. 11925501 and 12075048), and the Fundament Research Funds for the Central Universities (Grant No. DUT22ZD215).

References

[1] Chen W and Wang Z X 2020 *Chin. Phys. Lett.* **37** 125001
[2] Miao Y, Hao G Z, Liu Y, He H D, Chen W, Wang Y Q, Wang A K and Xu M 2021 *Chin. Phys. Lett.* **38** 085202
[3] Zhang H and Ma Z 2023 *Plasma Sci. Technol.* **25** 045105
[4] Cai H and Li D 2022 *Natl. Sci. Rev.* **9** nwac019
[5] Ren Z, Liu J, Wang F, Cai H, Wang Z and Shen W 2020 *Plasma Sci. Technol.* **22** 065102
[6] Shi H, Zhang W, Dong C, Bao J, Lin Z, Cao J and Li D 2020 *Chin. Phys. Lett.* **37** 085201
[7] Sun W, Wang J, Wei L, Wang Z, Liu D and He Q 2022 *Chin. Phys. B* **31** 110203
[8] Wang H, Wang Z X, Liu T and Zhu X L 2023 *Chin. Phys. Lett.* **40** 075201
[9] Fitzpatrick R 1995 *Phys. Plasmas* **2** 825
[10] Bickerton R J, Connor J W and Taylor J B 1971 *Nat. Phys. Sci.* **229** 110
[11] Chang Z, Callen J D, Fredrickson E D, Budny R V, Hegna C C, McGuire K M and Zarnstorff M C 1995 *Phys. Rev. Lett.* **74** 4663
[12] JET Team 1999 *Nucl. Fusion* **39** 1965
[13] Gude A, Günter S, Maraschek M, Zohm H and the ASDEX Upgrade Team 2002 *Nucl. Fusion* **42** 833
[14] Isayama A, Kamada Y, Ozeki T, Ide S, Fujita T, Oikawa T, Suzuki T, Neyatani Y, Isei N, Hamamatsu K, Ikeda Y, Takahashi K, Kajiwara K and JT-60 Team 2001 *Nucl. Fusion* **41** 761
[15] La Haye R J, Lao L L, Strait E J and Taylor T S 1997 *Nucl. Fusion* **37** 397
[16] Ji X Q, Yang Q W, Liu Y, Zhou J, Feng B B and Yuan B S 2010 *Chin. Phys. Lett.* **27** 065202
[17] Shi T, Wan B, Shen B, Sun Y, Qian J, Hu L, Gong X, Liu G, Luo Z, Zhong G, Xu L, Zhang J, Lin S, Jie Y, Wang F and Lv B 2013 *Plasma Phys. Control. Fusion* **55** 055007
[18] Buttery R J , Günter S, Giruzzi G, Hender T C, Howell D, Huysmans G, La Haye R J, Maraschek M, Reimerdes H, Sauter O, Warrick C D, Wilson H R and Zohm H 2000 *Plasma Phys. Control. Fusion* **42** B61
[19] La Haye R J 2006 *Phys. Plasmas* **13** 055501
[20] Sauter O, Henderson M A, Ramponi G, Zohm H and Zucca C 2010 *Plasma Phys. Control. Fusion* **52** 025002
[21] Jiang S, Tang W, Wei L, Liu T, Xu H and Wang Z 2022 *Plasma Sci. Technol.* **24** 055101
[22] Liu T, Wang Z X, Wei L and Wang J 2022 *Nucl. Fusion* **62** 056018
[23] Liu T, Wei L, Wang F and Wang Z X 2021 *Chin. Phys. Lett.* **38** 045204
[24] Tang W, Wei L, Wang Z, Wang J, Liu T and Zheng S 2019 *Plasma Sci. Technol.* **21** 065103
[25] Wang Z X, Tang W and Wei L 2022 *Plasma Sci. Technol.* **24** 033001
[26] Wang Z X, Liu T and Wei L 2022 *Rev. Mod. Plasma Phys.* **6** 14
[27] Günter S, Gude A, Maraschek M, Yu Q and the ASDEX Upgrade Team 1999 *Plasma Phys. Control. Fusion* **41** 767
[28] Bardoczi L, Logan N C and Strait E J 2021 *Phys. Rev. Lett.* **127** 055002
[29] Baruzzo M, Alper B, Bolzonella T, Brix M, Buratti P, Challis C D, Crisanti F, de la Luna E, de Vries P C, Giroud C, Hawkes N C, Howell D F, Imbeaux F, Joffrin E, Koslowski H R, Litaudon X, Mailloux J, Sips A C C and Tudisco O 2010 *Plasma Phys. Control. Fusion* **52** 075001
[30] He Y, Wang N, Ding Y, Li D, Zhou S, Mao F, Shen C, Jia R, Ren Z, Gao Y, Zhang Z, Li S, Huang Z, Chen H, Zhao C, Bala A A, Zhang W, Xie X, Chen Z, Yang Z, Chen Z, Yu Q and Pan Y 2023 *Plasma Phys. Control. Fusion* **65** 035012
[31] Sauter O, Buttery R J, Felton R, Hender T C, Howell D F and the EFDA-JET Workprogramme 2002 *Plasma Phys. Control. Fusion* **44** 1999
[32] Yu Q 2007 *Nucl. Fusion* **47** 1244
[33] Li D and Huo Y 1994 *Phys. Plasmas* **1** 315
[34] Yu Q, Günter S, Lackner K, Gude A and Maraschek M 2000 *Nucl. Fusion* **40** 2031
[35] Yu Q, Günter S and Lackner K 2000 *Phys. Rev. Lett.* **85** 2949
[36] Chandra D, Agullo O, Benkadda S, Garbet X and Sen A 2013 *Phys. Plasmas* **20** 042505
[37] Wei L, Wang Z X, Wang J and Yang X 2016 *Nucl. Fusion* **56** 106015
[38] Liu T, Wang J, Wei L and Wang Z X 2020 *Nucl. Fusion* **60** 106009
[39] Koslowski H R, Westerhof E, Bock M D, Classen I, Jaspers R, Kikuchi Y, Krämer-Flecken A, Lazaros A, Liang Y, Löwenbrück K, Varshney S, Hellermann M V, Wolf R, Zimmermann O and the TEXTOR team 2006 *Plasma Phys. Control. Fusion* **48** B53
[40] De Bock M F M, Classen I G J, Busch C, Jaspers R J E, Koslowski H R and the TEXTOR Team 2008 *Nucl. Fusion* **48** 015007
[41] Yu Q, Günter S and Lackner K 2021 *Nucl. Fusion* **61** 036040
[42] Yu Q 2010 *Nucl. Fusion* **50** 025014
[43] Fitzpatrick R 2018 *Phys. Plasmas* **25** 112505
[44] Hu Z Q, Ye C, Wei L and Wang Z X 2020 *Phys. Plasmas* **27** 012504
[45] Tang W, Luan Q, Sun H, Wei L, Lu S, Jiang S, Xu J and Wang Z 2023 *Plasma Sci. Technol.* **25** 045103
[46] Zhang W, Ma Z W and Wang S 2017 *Phys. Plasmas* **24** 102510
[47] Zhang W, Ma Z W and Zhang H W 2021 *Nucl. Fusion* **61** 126052
[48] Aiba N, Chen X, Osborne T H and Burrell K H 2023 *Nucl. Fusion* **63** 042001
[49] Hazeltine R D, Kotschenreuther M and Morrison P J 1985 *Phys. Fluids* **28** 2466
[50] Sato M and Wakatani M 2005 *Nucl. Fusion* **45** 143
[51] Glasser A H, Greene J M and Johnson J L 1975 *Phys. Fluids* **18** 875
[52] Lütjens H, Luciani J F and Garbet X 2001 *Plasma Phys. Control. Fusion* **43** A339
[53] Glasser A H, Greene J M and Johnson J L 1976 *Phys. Fluids* **19** 567
[54] Lütjens H and Luciani J-F 2002 *Phys. Plasmas* **9** 4837
[55] Urso L, Maraschek M, Zohm H and ASDEX Upgrade Team 2005 *J. Phys.: Conf. Series* **25** 266
[56] Hu Q M, Nazikian R, Chen X, Yu Q, Austin M E, Bortolon A, Ernst D, Haskey S R, Park J K, Yan Z and Yu G Y 2023 *Phys. Plasmas* **30** 020701
[57] Ye C, Wang Z X, Wei L and Hu Z Q 2019 *Nucl. Fusion* **59** 096044
[58] Paz-Soldan C, Hu Q, Logan N C and Park J K 2022 *Nucl. Fusion* **62** 126007
[59] Nazikian R, Hu Q, Ashourvan A, Eldon D, Evans T E, Grierson B A, Logan N C, Orlov D M, Park J K, Paz-Soldan C, Poli F M and Yu Q 2021 *Nucl. Fusion* **61** 044001
[60] Hu Q M, Nazikian R, Grierson B A, Logan N C, Orlov D M, Paz-Soldan C and Yu Q 2020 *Phys. Rev. Lett.* **125** 045001